ARL-TR-9264 ● Aug 2021

DEVCOM ARMY RESEARCH LABORATORY

Modeling the Nonlinear Behavior of UHMWPE Laminates Using Optimized Ply-Level Properties with Stepwise Fiber-Angle Rotations

by Jason J Cain, Jeffrey M Staniszewski, and Travis A Bogetti

NOTICES

Disclaimers

The findings in this report are not to be construed as an official Department of the Army position unless so designated by other authorized documents.

Citation of manufacturer's or trade names does not constitute an official endorsement or approval of the use thereof.

Destroy this report when it is no longer needed. Do not return it to the originator.

ARL-TR-9264 ● Aug 2021

Modeling the Nonlinear Behavior of UHMWPE Laminates Using Optimized Ply-Level Properties with Stepwise Fiber-Angle Rotations

Jason J Cain, Jeffrey M Staniszewski, and Travis A Bogetti
Weapons and Materials Research Directorate,
DEVCOM Army Research Laboratory

REPORT DOCUMENTATION PAGE

Form Approved
OMB No. 0704-0188

1. REPORT DATE *(DD-MM-YYYY)*	2. REPORT TYPE	3. DATES COVERED (From - To)
August 2021	Technical Report	Oct 1, 2018–Oct 1, 2019

4. TITLE AND SUBTITLE
Modeling the Nonlinear Behavior of UHMWPE Laminates Using Optimized Ply-Level Properties with Stepwise Fiber-Angle Rotations

5a. CONTRACT NUMBER

5b. GRANT NUMBER

5c. PROGRAM ELEMENT NUMBER

6. AUTHOR(S)
Jason J Cain, Jeffrey M Staniszewski, and Travis A Bogetti

5d. PROJECT NUMBER

5e. TASK NUMBER

5f. WORK UNIT NUMBER

7. PERFORMING ORGANIZATION NAME(S) AND ADDRESS(ES)
DEVCOM Army Research Laboratory
ATTN: FCDD-RLW-MA
Aberdeen Proving Ground, MD 21005

8. PERFORMING ORGANIZATION REPORT NUMBER
ARL-TR-9264

9. SPONSORING/MONITORING AGENCY NAME(S) AND ADDRESS(ES)

10. SPONSOR/MONITOR'S ACRONYM(S)

11. SPONSOR/MONITOR'S REPORT NUMBER(S)

12. DISTRIBUTION/AVAILABILITY STATEMENT
Approved for public release: distribution unlimited.

13. SUPPLEMENTARY NOTES
ORCID IDs: Jason J Cain, 0000-0003-2940-1361; Jeffrey M Staniszewski 0000-0002-2469-3257

14. ABSTRACT
Ultra-high-molecular-weight polyethylene (UHMWPE) composites are primarily designed for ballistic protection applications. The majority of UHMWPE composites combine a high specific-strength reinforcement with a compliant thermoplastic resin that generally results in a material with extreme anisotropy, large shear strain to failure, and high ballistic efficiency. This combination of properties makes it challenging to model UHMWPE composites analytically as they break some of the assumptions used in 3-D laminated media analysis. This report describes an iterative optimization methodology to determine the nonlinear ply-level response of UHMWPE composites. Several laminate configurations of two UHMWPE composite systems (Honeywell SpectraShield II SR-3136 and DuPont Tensylon HSBD 30A) are processed and tested under uniaxial tension for multiple loading angles. It is shown that accounting for strain-induced fiber-angle rotations is required to analytically model the laminates and determine the nonlinear ply-level response of both materials.

15. SUBJECT TERMS
ultra-high-molecular-weight polyethylene, composites, laminate analysis, nonlinear, ply-angle rotation

16. SECURITY CLASSIFICATION OF:			17. LIMITATION OF ABSTRACT	18. NUMBER OF PAGES	19a. NAME OF RESPONSIBLE PERSON
a. REPORT	b. ABSTRACT	c. THIS PAGE			Jason J Cain
Unclassified	Unclassified	Unclassified	UU	28	19b. TELEPHONE NUMBER (Include area code) (410) 306-0701

Contents

List of Figures

List of Tables

1. Introduction

Composites containing ultra-high-molecular-weight polyethylene (UHMWPE) fiber or film reinforcements have increasingly been studied for ballistic applications due to their superior performance.[1–5] The two most common forms of UHMWPE reinforced composites are 1) fiber-reinforced systems, where a high-volume fraction (typically >80%) of UHMWPE fibers are impregnated in a compliant, thermoplastic resin matrix and 2) film-reinforced systems, where thin sheets of highly aligned, solid-state extruded (SSE) UHMWPE films are bonded together and coated on one side with a thermoplastic binder resin. UHMWPE composites have several characteristics that create unique challenges in the processing and modeling of structures made from these materials. Due to the high amount of aligned material in both cases, a single lamina, or ply, of UHMWPE composite is generally highly anisotropic and very weak in the transverse direction. Manufacturers typically provide these materials in sheets containing 4 plies configured in a [0°/90°/0°/90°] orientation for fiber systems or 2 plies configured in a [0°/90°] orientation for film systems to facilitate handling during processing. This cross-ply configuration becomes the building block for potential stacking sequences in subsequent laminated composite structures.

In its simplest form, a UHMWPE composite structure is created when an unprocessed stack of material is consolidated at elevated temperature and pressure between two flat platens. In this case, the final orientation of the laminate is the same as its initial stacking sequence and its response is dependent on the process cycle used for consolidation. Processing UHMWPE composites into a structure with complex curvature is complicated by its resistance to shearing. To reduce wrinkling in the material and help the structure achieve a uniform thickness, a series of drawing or preforming steps at elevated temperature is generally used to form the part to its near-final shape before consolidation in matched metal molds.[6–9] The sheets of material are deformed and sheared during these manufacturing processes, causing deviation from the initial cross-ply architecture that can vary spatially within the part. The structural and ballistic responses of non-[0°/90°] laminates are fundamentally different from cross-ply configurations,[10] which can have a significant effect on the predicted response of these structures.

The ply-level response of UHMWPE materials is needed to develop accurate material models of the laminated composite response for use in finite element modeling, but experimental data on the ply-level properties are usually not available for most material systems as unidirectional (non-cross-ply) sheets may be difficult to obtain or process. A simple rule of mixtures assumption has be used to estimate the single-ply response for material model calibration for ballistic models

with some success.[11–13] The properties resulting from this assumption are linear, which is sufficient for the longitudinal behavior of most UHMWPE systems but generally insufficient for their transverse and shear response. The response of the matrix and reinforcement in state-of-the-art materials are typically unknown and their composition may be proprietary. Poor bonding between reinforcements and matrix in UHMWPE composites introduces additional complexities that are incompatible with an assumed rule of mixtures response.[11]

The approach to determine ply-level material properties taken in this report is based on 3-D laminated-media analysis. Unidirectional, ply-level material properties are calibrated through comparisons of predicted laminate response with experimental response for several laminate architectures. The nonlinear transverse and shear responses of experimental laminates are captured through a combination of assumed ply-level nonlinearity and fiber reorientation. A background of the laminated-media analysis, details on the processing of samples for the experiments, a description of the approach used to calibrate the properties, and discussions on the results are provided in the following sections.

2. Background

The response of laminates with a known layup and well-defined ply-level material behavior can be accurately predicted for small strains using 3-D laminated-media analysis.[14–17] This analysis, similar to Classical Laminated Plate Theory, was adapted to thick-section composite structures by accounting for through-thickness stresses and strains and neglecting bending–twisting coupling due to asymmetric layups. The analysis, originally developed by Chou et al.,[18] was modified to include nonlinear stress–strain behavior in all principal ply directions and progressive failure analysis by Bogetti et al.[19,20] and used to effectively predict the response and failure of various composites subjected to multiaxial loading. Predictions of the 3-D effective properties, effective laminate stress–strain response due to progressive ply failure, and ultimate strength for thick-section composite laminates under arbitrary mechanical loading are produced by an analytical code. A detailed description of the theory is available in the provided references and an overview of some of the relevant aspects are given in this section.

The Ramberg–Osgood equation is used to independently define nonlinear behavior in the longitudinal, or fiber, direction (1), in-plane transverse direction (2), transverse normal direction (3), interlaminar shear planes (23 and 13), and the in-plane shear plane (12). Figure 1 shows the relationship between the global (X, Y, Z), laminate-level ($\overline{X}$, $\overline{Y}$, $\overline{Z}$), and ply-level (1, 2, 3) coordinate systems. Note that $\overline{Z} = \left(\overline{X} \times \overline{Y}\right)$ and $3 = (1 \times 2)$.

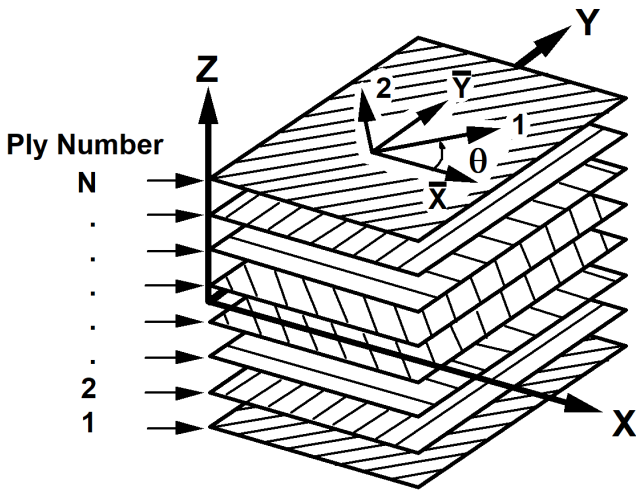

Fig. 1 Relationship between global (X, Y, Z), laminate-level ($\overline{X}$, $\overline{Y}$, $\overline{Z}$), and ply-level (1, 2, 3) coordinate systems

The Ramberg–Osgood equation provides an expression for ply-level stress written explicitly in terms of ply-level strain and three unique parameters:

$$\sigma = \frac{E_0 \varepsilon}{\left(1+\left(\frac{E_0 \varepsilon}{\sigma_0}\right)^n\right)^{\frac{1}{n}}} \tag{1}$$

Where E_o is the initial modulus, σ_0 is the asymptotic stress level, and n is a shape parameter for the stress-versus-strain curve. The instantaneous tangent lamina stiffness E_t is defined as a continuous function of ply-level strain and the three Ramberg–Osgood parameters by taking the derivative of Eq. 1 with respect to strain:

$$E_t = \frac{d\sigma}{d\varepsilon} = \frac{E_0}{\left(1+\left(\frac{E_0 \varepsilon}{\sigma_0}\right)^n\right)^{1+\frac{1}{n}}} \tag{2}$$

While the majority of nonlinear behavior in both structural and UHMWPE composites can be attributed to the response of the matrix, an additional contributor to nonlinearity observed in UHMWPE composites is the rotation, or scissoring, of reinforcements.[21–23] Modifications to the assumptions used in the laminated-media analysis are required to capture these deformation mechanisms, especially due to the large strains (>10%) seen in testing. An approach developed by Mandel et al.[24] is used to define the fiber rotation as a function of the current deformation state. The current ply angle θ_{i+1} is calculated using the relationship

$$\theta_{i+1} = \theta_i + \tan^{-1}\left(-\sin(\theta_i)\cos(\theta_i)\left(\Delta\overline{\varepsilon_X} - \Delta\overline{\varepsilon_Y}\right) + \frac{\Delta\overline{\varepsilon_{XY}}}{2}\left(\cos^2(\theta_i) - \sin^2(\theta_i)\right)\right) \tag{3}$$

where θ_i is the previous ply angle, and $\Delta\overline{\varepsilon_X}$, $\Delta\overline{\varepsilon_{XY}}$, and $\Delta\overline{\varepsilon_{XY}}$ are increments of laminate level strains in the $\overline{X}$, $\overline{Y}$, and in-plane shear directions, respectively.

The nonlinear response of the laminate is generated through the summation of piece-wise linear increments of stress over a pre-established load schedule. The tangent moduli and angle of each ply are used to determine the laminate stiffness matrix $\overline{C}$ for the calculation of the next laminate stress increment $\Delta\overline{\sigma}$ from the laminate strain increment $\Delta\overline{\varepsilon}$ as shown in Eq. 4:

$$\Delta\overline{\sigma} = \overline{C}\Delta\overline{\varepsilon} \tag{4}$$

The entire nonlinear response for the laminate is obtained by the cumulative sum of all stress and strain increments throughout the laminate loading history.

A complete description of ply-level material response is created from 21 mechanical constants. These constants include the three Ramberg–Osgood parameters for each of the six principal ply directions and the three major Poisson's ratios ν_{12}, ν_{13}, and ν_{23}. In this study, mechanical constants for a material model are calibrated for both fiber-based and film-based UHMWPE composite materials. A linear assumption is used to calibrate the initial modulus values, with nonlinear constants subsequently calibrated while including mechanisms of fiber rotation.

3. Experimental

3.1 Laminate Processing

The UHMWPE composites studied in this effort are laminated plates hot-pressed from commercially available thermoplastic composite sheet goods. Honeywell SpectraShield II SR-3136 (Honeywell International, Inc) and DuPont Tensylon HSBD 30A (DuPont de Nemours, Inc) are the two materials studied in this work. As received from the manufacturer, a sheet of SpectraShield II SR-3136 is composed of four unidirectional plies of gel-spun UHMWPE fibers impregnated with a thermoplastic polyurethane resin, with the plies oriented in a [0°/90°/0°/90°] configuration. A sheet of Tensylon HSBD 30A is composed of two orthogonally oriented unidirectional plies ([0°/90°]) of SSE UHMWPE film bonded together and coated on one side with a thermoplastic binder resin.

For both materials, laminates are processed from stacks of 45.72- × 45.72-cm (18- × 18-inch) oriented sheets placed between two sheets of PTFE-coated release material,* then between two sheets of 2-mm (0.08-inch)-thick, 60D durometer

* PTFE = polytetrafluoroethylene (e.g., Teflon).

silicone-rubber sheets. The entire stack is placed into the female cavity of a custom-made, passively heated mold that provides lateral confinement of the rubber sheets to prevent outward extrusion of the materials during hot pressing. The male portion of the mold is placed on top and the laminate is then processed using a uniaxial hydraulic-ram hot press (Model 800H-48-BCLPX; Wabash MPI) with a maximum load capacity of 7.1 MN (800 tons) as shown in Fig. 2. The nominal processing pressure for both materials is 20.7 MPa (3000 psi), although their nominal processing temperatures are different: 132 °C for SpectraShield II SR-3136 and 110 °C for Tensylon HSBD 30A. Processing temperatures are measured using a thermocouple placed approximately 3-cm (1.18-inch) offset from one corner at the midplane of the laminate.

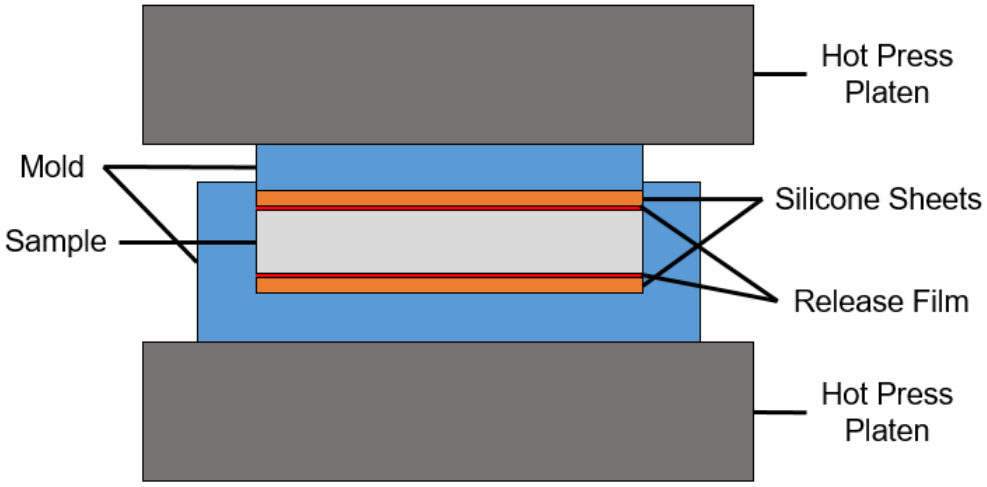

Fig. 2 Schematic of processing setup

The processing cycle used for these materials begins with the application of pressure equal to one-quarter of the nominal processing pressure until the measured laminate temperature reached 60 °C. Full pressure is then applied and the plate temperature is ramped up to the nominal processing temperature. Temperature and pressure are held uniform for 30 min, at which point the temperature is ramped down to ambient. Full pressure is held during the cool-down process until the plate temperature dropped below 35 °C to avoid uncontrolled thermomechanical material relaxation.

3.2 Sample Preparation and Testing

For each material, three laminates are created and specimens are tested in seven loading cases as shown in Table 1. The ply orientations listed correspond to the orientations of individual plies within the sheet, rather than to each sheet, with each layup containing 32 plies, created with 8 sheets of SpectraShield II SR-3136 or 16 sheets of Tensylon HSBD 30A. These test cases are expected to have a wide range in elastic moduli and were chosen as representative orientations that might be seen in a structure with complex curvature.

Table 1 Layups and loading directions of the test specimens

Designation	Layup	Loading direction
30/–30@0	$[(-30°/+60°)_2(+30°/-60°)_2]_{2s}$	0°
30/–30@30	$[(-30°/+60°)_2(+30°/-60°)_2]_{2s}$	30°
30/–30@45	$[(-30°/+60°)_2(+30°/-60°)_2]_{2s}$	45°
Quasi@0	$[(0°/90°)_2(+45°/-45°)_2]_{2s}$	0°
Quasi@22.5	$[(0°/90°)_2(+45°/-45°)_2]_{2s}$	22.5°
45/–45@0	$[(+45°/-45°)]_{4s}$	0°
45/–45@22.5	$[(+45°/-45°)]_{4s}$	22.5°

Tensile specimens are cut using a waterjet (OMAX MicroMAX; OMAX Corporation) using a water pressure of 379 MPa (55 ksi) and 200-grit garnet as the abrasive. Each specimen is cut into a dogbone geometry as shown in Fig. 3. The dogbone geometry was chosen after initial trials using straight-sided specimens found the outer plies of the specimen were stripped by the load-frame grips at relatively low loads, primarily due to the very low interlaminar shear strength of the materials. The dogbone geometry achieves complete loading to failure for layups and loading directions without plies aligned in the testing direction. For layups and loading directions with plies aligned in the testing direction, the stripping of outer plies before primary failure is delayed until a significant portion of the stress–strain curve is revealed.

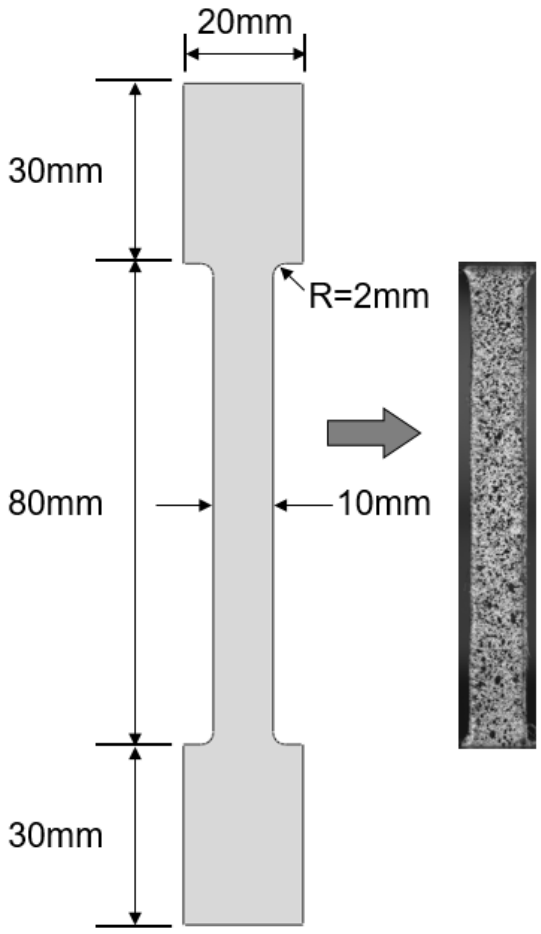

Fig. 3 Schematic of the dogbone specimen and an example of the speckle pattern used in the gauge section

Uniaxial tension is applied to the specimens at a displacement rate of 12.7 mm/min at room temperature. Strain is measured with 3-D digital image correlation (DIC) using a speckle pattern that is applied over the entire gauge length, as shown in Fig. 3. VIC-Snap 3D software (Correlated Solutions, Inc) is used to capture images from a pair of 3.2-megapixel cameras and a combined viewing angle of approximately 20°. VIC-3D software is used to correlate the results and export the axial strain data in the testing direction for the surface ply.

Experimental axial stress–strain curves for the five loading cases of the *30/–30* and *Quasi* laminates of SpectraShield II SR-3136 are shown in Fig. 4. Five samples were tested for each loading case and their responses were very repeatable, so a single representative curve is shown for each case. The response for these test cases included a stress peak, followed by a gradual or sudden drop in stress. The portion of the curve beyond the stress peak was assumed to include delamination and other

forms of ply-level and laminate-level damage accumulation. As these mechanisms were not included in analytical model predictions, only experimental data up to the peak stress were used for comparisons. An explanation of the linear and nonlinear analytical predictions shown in this and subsequent figures is given in the following section.

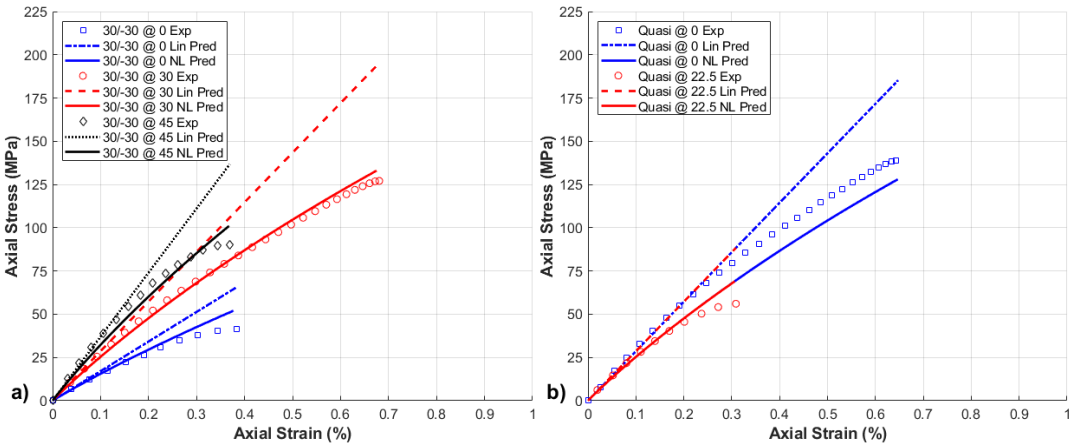

Fig. 4 Experimental and predicted stress–strain curves of SpectraShield II SR-3136 for a) *30/–30* and b) *Quasi* load cases

Experimental axial stress–strain curves for the two loading cases of the *45/–45* SpectraShield II SR-3136 laminates are shown in Fig. 5a. For the *45/–45@0* loading case, a comparison between the rotations of reinforcements on the surface of tensile coupons extracted from the DIC data and the fiber rotation predicted by the model as a function of laminate axial strain is also included in Fig. 5b.

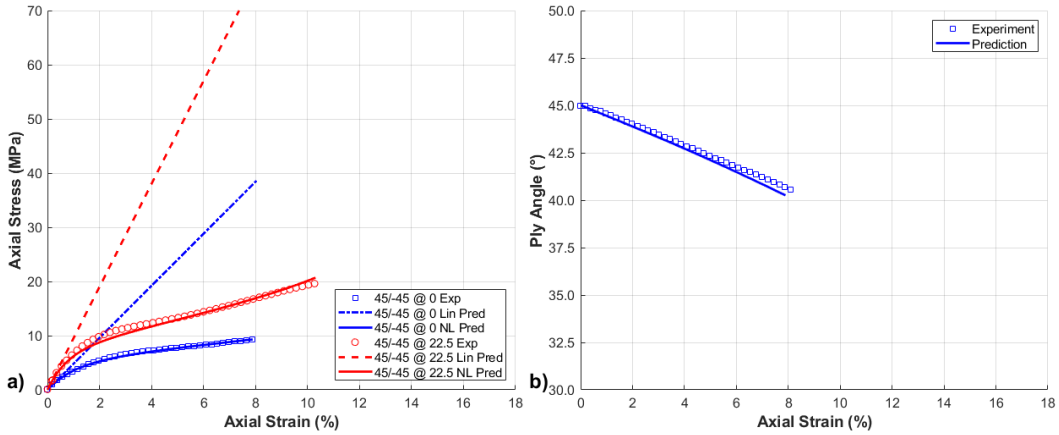

Fig. 5 Experimental and predicted data of *45/–45* loading cases of SpectraShield II SR-3136 a) axial stress–strain curves and b) surface ply angle vs. strain

Experimental data for Tensylon HSBD 30A is shown in Fig. 6 for the five loading cases of the *30/–30* and *Quasi* laminates and Fig. 7 for the two loading cases of the *45/–45* laminates. Similar to the SpectraShield II SR-3136 response, peak loading for the *30/–30* and quasi-isotropic laminates occurs at very low axial strains (<1%) while the *45/–45* laminates achieve significantly higher failure strains. The compliance of the matrix and reorientation of the reinforcements in the *45/–45* laminates contribute to the increased strain capacity of these materials.

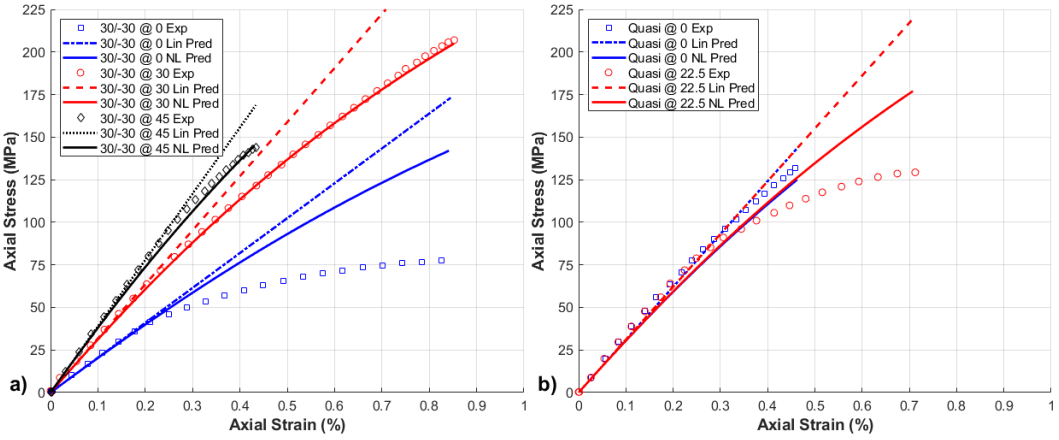

Fig. 6 Experimental and predicted stress–strain curves of Tensylon HSBD 30A for a) *30/–30* and b) *Quasi* load cases

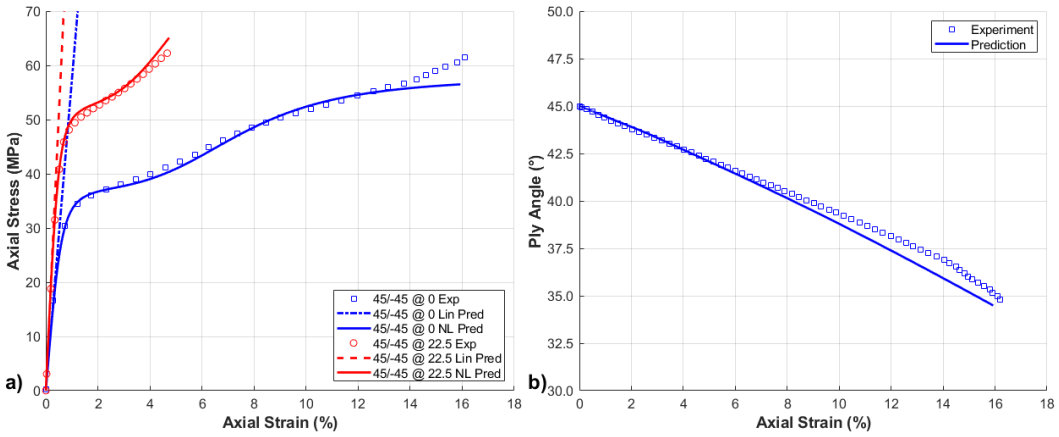

Fig. 7 Experimental and predicted data of *45/–45* loading cases of Tensylon HSBD 30A a) axial stress–strain curves and b) surface ply angle vs. strain

4. Calibration of Mechanical Constants

4.1 Methodology

The development of ply-level material properties for UHMWPE composites that can successfully predict the response of arbitrary laminates could significantly improve the accuracy of material models used in structural and ballistic simulations. The ply-level material properties of SpectraShield II SR-3136 and Tensylon HSBD 30A are developed in this report by using an iterative approach incorporated into a custom MATLAB code that finds the best overall fit between experiment and prediction for all of the laminates and loading directions considered. Initially, upper and lower bounds for each Ramberg–Osgood parameter are chosen such that it is certain the true value of each parameter will lie within the limits. These bounds define the outer limits of a coarse grid containing five grid nodes in each direction of the parameter space. The analytical code is used to predict the response of each laminate and loading direction (seven total) at each node point. To refine the estimate, a new grid with one-half of the spacing of the previous grid, centered on the previous generation's "optimal" point, is defined and evaluated. This grid refinement is executed iteratively until the difference between the "optimal" material properties in each direction for two successive iterations is less than 1%.

4.2 Linear-Elastic Assumption

The initial ply-level stiffness parameters are first calibrated to the experimental laminate moduli for the seven loading cases using the assumption of a linear-elastic ply-level response. The nine linear-elastic mechanical constants (six elastic moduli

and three Poisson's ratios) were first separately varied between their upper and lower bounds to estimate the individual effect of the constant on the predicted initial laminate modulus. This screening procedure found the mechanical constants E_1, E_2, G_{12}, and ν_{12} were the most influential parameters for the initial laminate modulus predictions. The in-plane Poisson's ratio ν_{12} is the least significant of these parameters and was assigned a value of 0.3 to further simplify the analysis.

The iterative approach described previously is used to calibrate the elastic constants to the experimental response. The sum of the absolute error, or total error, across the seven load cases shown in Eq. 5 is used to determine the optimal point in the E_1–E_2–G_{12} parameter space:

$$\epsilon_T = \sum_{i=1}^{7} \frac{|E_e^i - E_p^i|}{E_e^i} \tag{5}$$

where E_e and E_p are the initial moduli of the experimental and predicted laminate stress–strain curves for the i^{th} case, respectively.

Table 2 lists the initial upper and lower bounds and the subsequent calibrated value for both SpectraShield II SR-3136 and Tensylon HSBD 30A. SpectraShield II SR-3136 has an optimal initial longitudinal stiffness of 78.9 GPa and an initial shear stiffness of 121 MPa. These values are consistent with ply-level properties used in simulations of other fiber-reinforced UHMWPE composite materials, such as Dyneema HB26.[13,25–28] The longitudinal stiffness is also in the range of values calculated from a simple rule of mixtures for a fiber-volume fraction of 83% and a fiber stiffness of 95 GPa. The initial longitudinal modulus of 83.4 GPa for Tensylon HSBD 30A is close to the reported value of 88 GPa.[29–31] It should be noted the value chosen for E_2 has very little effect on the total error determined at any given point for either material and thus the values of E_2 listed here are subject to significant uncertainty.

Table 2 Calibrated ply-level elastic moduli for longitudinal, transverse, and shear directions

Input	SpectraShield II SR-3136			Tensylon HSBD 30A		
	Lower bound (GPa)	Upper bound (GPa)	Optimal value (GPa)	Lower bound (GPa)	Upper bound (GPa)	Optimal value (GPa)
E_1	55.2	110.3	78.9	55.2	110.3	83.4
E_2	3.4	13.8	7.5	3.4	13.8	6.21
G_{12}	0.0345	0.276	0.121	0.500	5.00	1.52

Figure 8 compares the experimentally measured laminate moduli with analytically predicted values for each material and loading case. The calibrated input values provide a very good agreement across all seven loading cases for both materials.

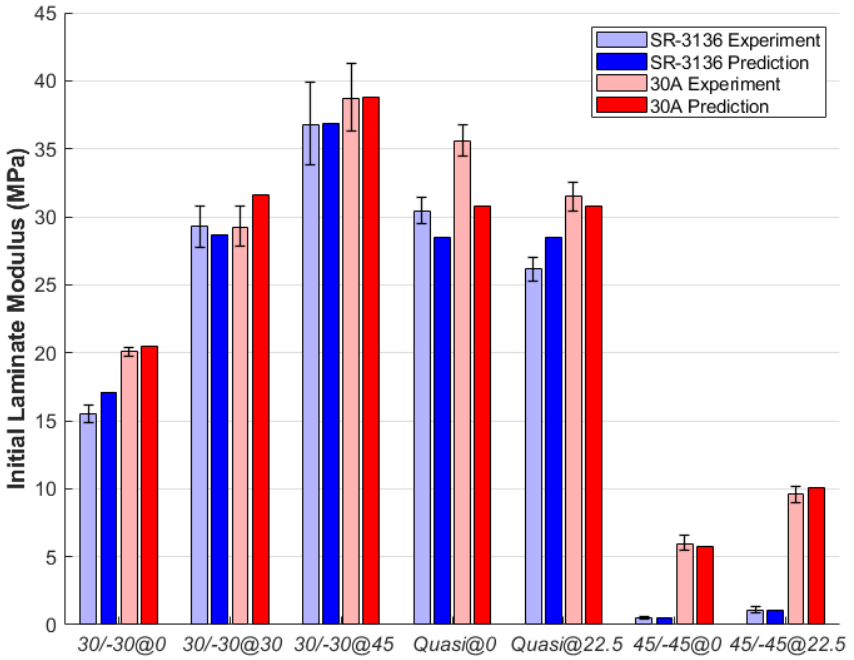

Fig. 8 Experimental and predicted laminate initial modulus values for seven loading cases of SpectraShield II SR-3136 and Tensylon HSBD 30A

Laminate modulus varies as a function of loading direction depending on the layup and the ply-level response of the material. Both SpectraShield II SR-3136 and Tensylon HSBD 30A exhibit a high degree of ply-level anisotropy, which is apparent in the laminate moduli produced by the layup and loading directions. Figures 9 and 10 show the change in laminate modulus predictions as a function of loading angle along with comparisons with experimental modulus for the three tested laminates for SpectraShield II SR-3136 and Tensylon HSBD 30A, respectively. The cases designated as *30/–30* (a $[(–30°/+60°)_2(+30°/–60°)_2]$ layup)

were found to have their lowest modulus in the 0° loading direction and their highest modulus in the 45° loading direction as predicted by the analysis. Quasi-isotropic layups produce the same modulus irrespective of loading direction and this is reflected in the experimental results of the chosen loading directions. The modulus of *45/–45* laminates varies the most with loading angle as the lowest predicted modulus is in the 0° direction and the highest is along the direction of half of the fibers in the 45° direction. The weak laminate response of both materials for these cases is therefore in line with the theoretical predictions. These results show the initial modulus of UHMWPE composite laminates with general layups can be accurately predicted using laminated-media analysis.

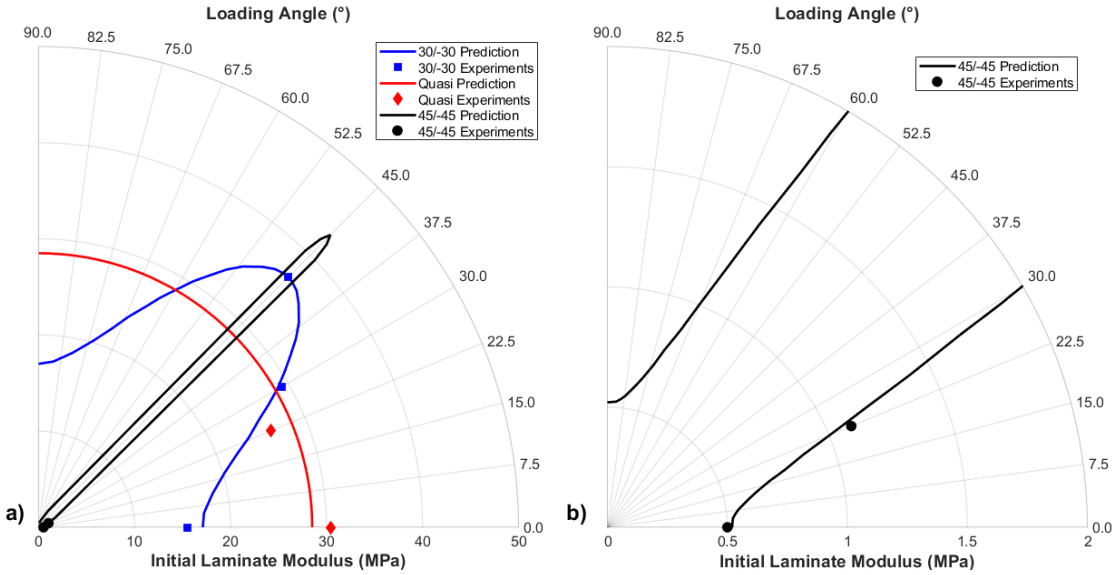

Fig. 9 Polar plots comparing axial modulus predictions with experimental values of SpectraShield II SR-3136 for *30/–30*, *Quasi*, and *45/–45* cases a) all cases and b) detailed plot highlighting *45/–45* results

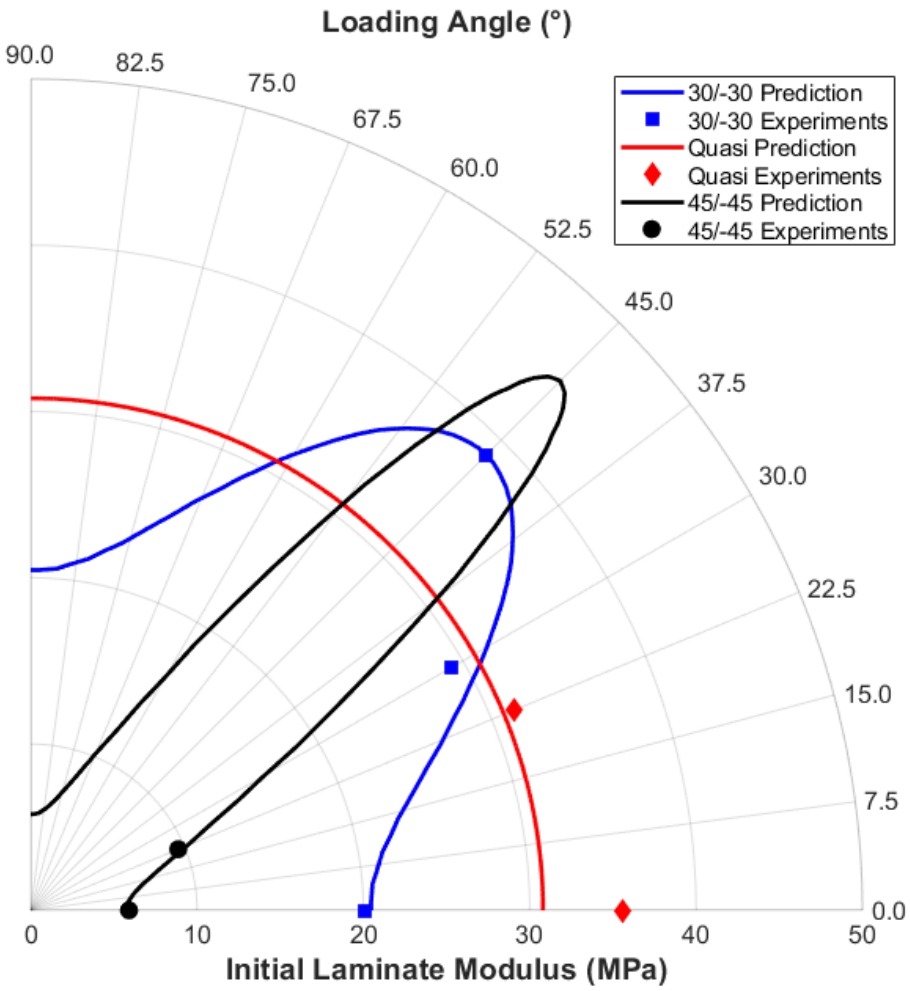

Fig. 10 Polar plots comparing axial modulus predictions with experimental values of Tensylon HSBD 30A for *30/–30*, *Quasi*, and *45/–45* cases

4.3 Calibration of Nonlinear Parameters

The linear analysis has established calibrated values for the initial ply-level modulus parameters in the longitudinal, transverse, and in-plane shear directions. The next objective is to calibrate the additional nonlinear parameters of the Ramberg–Osgood relationship for these materials. The through-thickness and out-of-plane shear parameters along with the out-of-plane Poisson's ratios for these materials were identified by another screening procedure as insignificant contributors to the in-plane laminate response and were discarded from the analysis. The remaining factors are the stress asymptotes and shape factors of the longitudinal, transverse, and in-plane shear directions ($\sigma_{0,E1}$, η_{E1}, $\sigma_{0,E2}$, η_{E2}, $\sigma_{0,G12}$, and η_{G12}, respectively).

The correlation between the experimental and predicted response is measured using the root-mean-squared-error (RMSE) as defined in Eq. 6:

$$RMSE = \sqrt{\frac{\sum_{t=1}^{T}(\hat{y}_t - y_t)^2}{T}} \quad (6)$$

where $\hat{y}_t$ is the predicted laminate stress at a given laminate strain, t; y_t is the experimental value at that same strain; and T is number of points in the curve. The predicted stress–strain curves are linearly interpolated to match the amount of experimental data points for the RMSE calculation.

Similar to the linear analysis, the nonlinear analysis is designed to iterate through material property values along independent axes in the corresponding parameter space, in this case a 6-D space. None of the loading cases for the laminates are influenced by all of the parameters. The nonlinear parameters associated with E_1 have a strong effect on stress–strain predictions for five cases (*30/–30@0, 30/–30@30, 30/–30@45, Quasi@0, and Quasi@22.5*), with the E_2 and G_{12} parameters having a small contribution. The reverse is true for the remaining two cases (*45/–45@0* and *45/–45@22.5)*. To reduce computation time, the four nonlinear parameters associated with E_2 and G_{12} are first found using the two *45/–45* cases with the linear longitudinal assumption of $\sigma_{0,E1} = 10$ GPa and $\eta_{E1} = 1$. The remaining five cases are then used to calibrate E_1 nonlinear parameters using the optimized transverse and shear parameters. The results of the calibration of the nonlinear parameters are shown in Table 3 for each material.

Table 3 Initial bounds and optimized values for nonlinear Ramberg–Osgood parameters

Input	SpectraShield II SR-3136			Tensylon HSBD 30A		
	Lower bound	Upper bound	Optimal value	Lower bound	Upper bound	Optimal value
$\sigma_{0,E2}$	7 MPa	70 MPa	24.1 MPa	10 MPa	140 MPa	59.8 MPa
η_{E2}	0.1	10	0.525	0.1	10	1.42
$\sigma_{0,G12}$	1 MPa	50 MPa	3.96 MPa	1 MPa	50 MPa	18.1 MPa
η_{G12}	0.1	10	1.20	0.1	10	2.25
$\sigma_{0,E1}$	0.1 GPa	50 GPa	0.92 GPa	0.1 GPa	50 GPa	1.59 GPa
η_{E1}	0.1	10	0.93	0.1	10	1.07

5. Discussions

Figure 4 shows the predicted laminate response versus the experimental data for the three *30/–30* and two *Quasi* cases for SpectraShield II SR-3136. Although the calibrated linear properties provide accurate predictions of initial laminate modulus (<0.1% strain), the inclusion of nonlinearity is required to predict the actual response of the laminate up until its peak load. The predicted nonlinear response of

the *Quasi* laminates are the same for both loading cases as any effects from fiber rotations are minimal at these strain levels. The *Quasi@22.5* experimental response begins to deviate from both the predicted response and the *Quasi@0* case at a relatively small strain. It is suspected in this region that the specimen is experiencing mechanisms associated with failure initiation, such as delamination, ply-level shear failure (splitting), and so on, and the analytical model is not expected to correctly predict laminate response after failure has begun.

Similar mechanisms can be seen in the *30/–30@0* and *Quasi@22.5* cases of Tensylon HSBD 30A shown in Fig. 6. The loading direction of the *Quasi@0* case engages 25% of the plies in the axial direction, while transverse and shear loading of the plies are more prevalent for the *Quasi@22.5* and *30/–30@0* cases. The analytical model provides a better correlation with experiments for both materials in loading cases where the axial response of the ply has a greater influence (*30/–30@30*, *30/–30@45*, and *Quasi@0*).

Comparisons of experimental data and predicted axial laminate strain for the *45/–45@0* and *45/–45@22.5* cases are shown in Figs. 5 and 7 for SpectraShield II SR-3136 and Tensylon HSBD 30A, respectively. These predictions, which include the temporary assumption of linearity in the longitudinal direction, are in very good agreement with the experiments for both materials. The ply-level, nonlinear shear response is calibrated with the assumption of fiber rotation during deformation. DIC on the surface of *45/–45@0* samples shows significant reorientation of the fibers for both materials (Figs. 5b and 7b). The inclusion of fiber-rotation mechanics is therefore critical to accurately predict the response of these laminates.

A comparison of the predicted response of the two *45/–45* load cases both with and without the effects of fiber rotations are shown in Fig. 11. The predicted response of the laminates without fiber-rotation mechanisms significantly underestimates the experimental data. The experimental results show the laminates softening at lower strains before stiffening as the fibers begin to reorient toward the direction of loading. This softening–stiffening response could not be captured directly using only the Ramberg–Osgood equation. Calibration of the ply-level nonlinear 12-shear response without the inclusion of fiber-rotation mechanisms would lead to an overly stiff response, affecting the predictions of other laminate configurations, and ultimately adversely impacting the calibrated input parameters of the other principal directions.

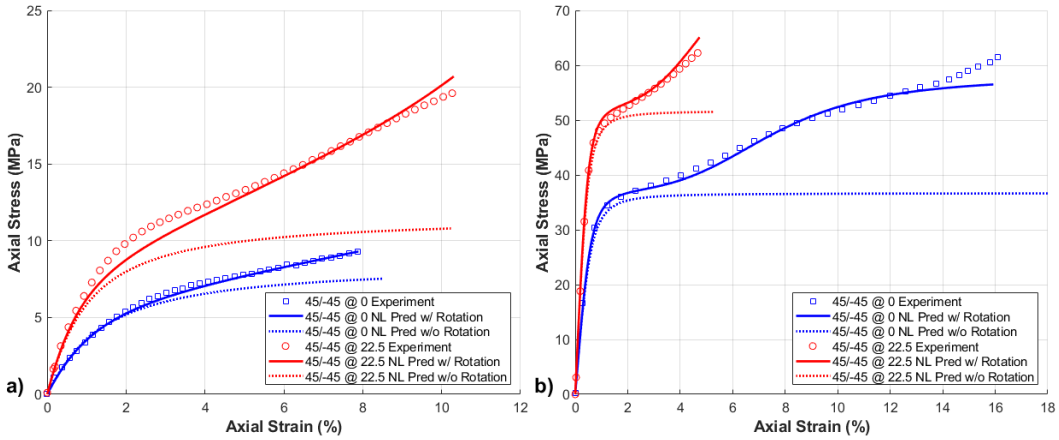

Fig. 11 Comparisons of experimental data and nonlinear analytical model predictions with and without effects of fiber rotations for both *45/–45* loading cases of a) SpectraShield II SR-3136 and b) Tensylon HSBD 30A

6. Conclusions

A number of UHMWPE laminate architectures were fabricated from Honeywell SpectraShield II SR-3136 and DuPont Tensylon HSBD 30A and tested in uniaxial tension. An iterative optimization algorithm was used to compare analytical model predictions with experimental data to calibrate nonlinear material inputs. This approach was first used to find linear ply-level material properties (E_1, E_2, and G_{12}) assuming infinitesimal strains and no fiber rotations. It was then extended to the case of finite laminate strains with nonlinear material properties and finite fiber rotations. An optimized set of material property inputs was found for each material that resulted in the minimum possible cumulative error between model and experimental data across a total of seven test cases. The iterative optimization algorithm produced linear material properties consistent with independent assessments of these properties through other testing methodologies and were consistent with values found in the literature. The analytical model successfully predicted the small-strain, linear uniaxial laminate response for both a typical gel-spun UHMWPE fiber material and for an SSE UHMWPE film material system. The material and geometric nonlinear response of the composite systems were also well predicted up to the point of ply- and laminate-level damage initiation. These results demonstrate that ply-level properties can be extracted from the experimental response of complex laminate architectures of UHMWPE composites using laminated-media theory with accommodations for ply angle reorientation. More significantly, this approach can potentially be used with analytical and finite element modeling to design UHMWPE laminated composite architectures to meet specific structural, low velocity, and ballistic impact requirements, which are the subject of future investigations.

7. References

1. Zhang TG, Satapathy SS, Vargas-Gonzalez LR, Walsh SM. Ballistic impact response of ultra-high-molecular-weight polyethylene (UHMWPE). Compos Struct. 2015;133:191–201.
2. Attwood J, Russell B, Wadley H, Deshpande V. Mechanisms of the penetration of ultra-high molecular weight polyethylene composite beams. Int J Impact Eng. 2016;93:153–165.
3. Alil L, Arrigoni M, Badea S, Ginghină R, Matache L, Mostovykh P. Ballistic study of Tensylon®-based panels. Express Polym Lett. 2018;12(6):491–504.
4. Lässig TR, May M, Heisserer U, Riedel W, Bagusat F, van der Werff H, Hiermaier SJ. Effect of consolidation pressure on the impact behavior of UHMWPE composites. Compos Part B-Eng. 2018;147:47–55.
5. Zulkifli F, Stolk J, Heisserer U, Yong AT-M, Li Z, Hu XM. Strategic positioning of carbon fiber layers in an UHMwPE ballistic hybrid composite panel. Int J Impact Eng. 2019;129:119–127.
6. Campbell DT, Cramer DR. Hybrid thermoplastic composite ballistic helmet fabrication study. Society for the Advancement of Material and Process Engineering. Fiberforge Corporation; 2008.
7. Folgar F. Thermoplastic matrix combat helmet with carbon-epoxy skin for ballistic performance. In: Chen X, editor. Advanced Fibrous Composite Materials for Ballistic Protection. Woodhead Publishing; 2016. p. 437–456.
8. Dangora LM, Mitchell CJ, Sherwood J, Parker JC. Deep-drawing forming trials on a cross-ply thermoplastic lamina for helmet preform manufacture. J Manuf Sci Eng. 2017;139(3).
9. Giray M, Bailey S. Developments in lightweight composite ballistic helmet manufacture. Güvenlik Bilimleri Dergisi. 2019;79–94.
10. Ansari B, Kawashita L, Hallett S, Heisserer U. Manufacture and ballistic testing of sheared plates made from Dyneema HB26®. AuxDefense 2018: 1st World Conference on Advanced Materials for Defense; 2018.
11. Iannucci L, Del Rosso S, Curtis P, Pope D, Duke P. Understanding the thickness effect on the tensile strength property of Dyneema® HB26 laminates. Materials. 2018;11(8):1431.

12. Hazzard MK, Curtis PT, Iannucci L, Hallett S, Trask R. An investigation of in-plane performance of ultra-high molecular weight polyethylene composites. 20th International Conference on Composite Materials; 2015. p. 19–24.

13. Hazzard MK, Trask RS, Heisserer U, Van Der Kamp M, Hallett SR. Finite element modelling of Dyneema® composites: from quasi-static rates to ballistic impact. Compos Part A-Appl S. 2018;115:31–45.

14. Bogetti TA, Hoppel CP, Harik VM, Newill JF, Burns BP. Predicting the nonlinear response and progressive failure of composite laminates. Compos Sci Technol. 2004;64(3–4):329–342.

15. Bogetti TA, Hoppel CP, Harik VM, Newill JF, Burns BP. Predicting the nonlinear response and failure of composite laminates: correlation with experimental results. In: Hinton MJ, Kaddour AS, Soden PD, editors. Failure Criteria in Fibre-Reinforced-Polymer Composites: The World-Wide Failure Exercise. Elsevier; 2004. p. 961–975.

16. Bogetti TA, Staniszewski J, Burns BP, Hoppel CP, Gillespie Jr JW, Tierney J. Predicting the nonlinear response and progressive failure of composite laminates under tri-axial loading. J Compos Mater. 2012;46(19–20):2443–2459.

17. Bogetti TA, Staniszewski J, Burns BP, Hoppel CP, Gillespie Jr JW, Tierney J. Predicting the nonlinear response and progressive failure of composite laminates under triaxial loading: correlation with experimental results. J Compos Mater. 2013;47(6–7):793–804.

18. Chou P, Carleone J, Hsu C. Elastic constants of layered media. J Compos Mater. 1972;6(1):80–93.

19. Bogetti TA, Hoppel CP, Burns BP. LAMPAT: a software tool for analyzing and designing thick laminated composite structures. Army Research Laboratory (US); 1995 Sep. Report No.: ARL-TR-890.

20. Bogetti TA, Hoppel CP, Drysdale WH. Three-dimensional effective property and strength prediction of thick laminated composite media. Army Research Laboratory (US); 1995 Oct. Report No.: ARL-TR-911.

21. Cline J, Yeager M, Bogetti T. Determination of in-plane shear properties of ultra-high-molecular-weight polyethylene (UHMWPE) composites for input into a thermoforming model. Army Research Laboratory; 2019 Aug. Report No: ARL-TR-8769.

22. White K, Yeager M, Sherwood J, Bogetti T, Cline J. Material characterization and finite element modeling for the forming of highly oriented UHMWPE thin-film and unidirectional cross-ply composites. In: Waas A, editor. Proceedings of the 33rd ASC Technical Conference; 2018.

23. Yeager M, Bogetti T. Single curvature preforming of ultra-high molecular weight polyethylene (UHMWPE) composites. Army Research Laboratory; 2019 Sep. Report No.: ARL-TR-8778.

24. Mandel U, Taubert R, Hinterhölzl R. Mechanism based nonlinear constitutive model for composite laminates subjected to large deformations. Compos Struct. 2015;132:98–108.

25. Hazzard MK, Hallett S, Curtis PT, Iannucci L, Trask RS. Effect of fibre orientation on the low velocity impact response of thin Dyneema® composite laminates. Int J Impact Eng. 2017;100:35–45.

26. Liu G, Thouless MD, Deshpande VS, Fleck NA. Collapse of a composite beam made from ultra high molecular-weight polyethylene fibres. J Mech Phys Solids. 2014;63:320–335.

27. Liu G. Modelling microbuckling failure of a composite cantilever beam made from ultra high molecular-weight polyethylene fibres. Acta Mech. 2015;226(4):1255–1266.

28. Liu G, Zhu W, Huang G. The microbuckling failure of Dyneema® composites under compression. Acta Mech Solida Sin. 2017;30(4):425–434.

29. Jordan ND, Olley RH, Bassett DC, Hine PJ, Ward IM. The development of morphology during hot compaction of Tensylon high-modulus polyethylene tapes and woven cloths. Polymer. 2002;43(12):3397–3404.

30. Orench IP, Calleja FB, Hine P, Ward I. A microindentation study of polyethylene composites produced by hot compaction. J Appl Polym Sci. 2006;100(2):1659–1663.

31. Hine PJ, Unwin AP, Ward IM. The use of an interleaved film for optimising the properties of hot compacted polyethylene single polymer composites. Polymer. 2011;52(13):2891–2898.

List of Symbols, Abbreviations, and Acronyms

3-D	three-dimensional
6-D	six-dimensional
DIC	digital image correlation
PTFE	polytetrafluoroethylene
RMSE	root-mean-squared-error
SSE	solid-state extruded
UHMWPE	ultra-high-molecular-weight polyethylene

1 (PDF) DEFENSE TECHNICAL INFORMATION CTR DTIC OCA

1 (PDF) DEVCOM ARL FCDD RLD DCI TECH LIB

19 (PDF) DEVCOM ARL FCDD RLW MA JJ CAIN TA BOGETTI JM STANISZEWSKI SE BOYD M YEAGER TA PLAISTED ED WETZEL RJ NEICE FCDD RLW MB DJ O'BRIEN FCDD RLW ME LR VARGAS-GONZALEZ FCDD RLW B CP HOPPEL RC BECKER AL TONGE PJ GILLICH FCDD RLW TB SS SATAPATHY TG ZHANG M KLEINBERGER FCDD RLW TF PA JANNOTTI CS MEYER

2 (PDF) PROG EXECUTIVE SOLDIER OFC DM OTTERSON AL DE GROOT

8 (PDF) DEVCOM NATICK SOLDIER SYSTEMS CTR RV DILALLA JC PARKER D KUBIAK CA HEWITT WS SHAW SA BENNETT CL LEWIS JA ORLANDO